Molecular Therapy
Nucleic Acids
Original Article

A combination of systemic mannitol and mannitol modified polyester nanoparticles for caveolae-mediated gene delivery to the brain

Betsy Reshma Gilbert,[1,2] Chirag Miglani,[3] Arundhati Karmakar,[4] Muneesh Pal,[1,2] Vysakh C. Chandran,[3] Sarika Gupta,[4] Asish Pal,[3] and Munia Ganguli[1,2]

[1]CSIR-Institute of Genomics and Integrative Biology, Mathura Road, New Delhi 110025, India; [2]Academy of Scientific and Innovative Research (AcSIR), Ghaziabad 201002, India; [3]Chemical Biology Unit, Institute of Nanoscience and Technology, Sector 81, Mohali, Punjab 140306, India; [4]National Institute of Immunology, New Delhi 110067, India

Overcoming the blood-brain barrier (BBB) remains a significant challenge for nucleic acid delivery to the brain. We have explored a combination of mannitol-modified poly (β-amino ester) (PBAE) nanoparticles and systemic mannitol injection for crossing the BBB. We incorporated mannitol in the PBAE polymer for caveolae targeting and selected monomers that may help avoid delivery to the liver. We also induced caveolae at the BBB through systemic mannitol injection in order to create an opportunity for the caveolae-targeting nanoparticles (M30 D90) containing plasmid DNA to cross the BBB. When a clinically relevant dose was administered intravenously in this caveolae induction model, M30 D90 demonstrated significant transgene expression of a reporter plasmid in the brain, with selective uptake by neuronal cells and minimal liver accumulation. We demonstrate that caveolae modulation using systemic mannitol administration and caveolae targeting using designed nanoparticles are necessary for efficient delivery to the brain. This delivery platform offers a simple, scalable, and controlled delivery solution and holds promise for treating brain diseases with functional targets.

INTRODUCTION

More than 1,000 central nervous system (CNS) diseases affect over 1 billion people globally.[1] Nucleic acid drugs with rich target selection present promising therapeutic alternatives for brain disorders that were previously deemed untreatable.[2] Unfortunately, multiple biological barriers prevent efficient nucleic acid delivery into the brain. The blood-brain barrier (BBB), considered the most important one, is a cellular dynamic barrier that protects the CNS from blood components. The barrier properties of the BBB arise from tight junctions between endothelial cells and a low transcytosis rate, which restricts the paracellular and intracellular movement of molecules.[3]

Several strategies have been developed over the years based on a molecular understanding of the BBB to facilitate the delivery of small and large molecules, viewing the BBB as an interface for delivery.[4,5] Much research focuses on active targeting approaches, with one or more targeting ligands attached to the delivery system to facilitate receptor-mediated transcytosis.[6,7] However, this increases the size and complexity of the delivery system. Moreover, the receptor expression is dynamic with age and disease, limiting the potential of these strategies.[8–10] Another approach is to modulate the BBB permeability with transient tight junction opening strategies. Antibodies and peptides against tight junction proteins,[11,12] intracarotid administration of hyperosmotic mannitol,[13] and focused ultrasound[14] have been utilized to deliver small molecules. Combining these two strategies has proven most effective for intravenously administered macromolecular cargoes, with studies showing that coupling delivery systems with focused ultrasound enables efficient transgene expression and genome editing.[15–17]

Recent literature suggests that the caveolae-mediated transcytosis pathway across the BBB represents a relatively unexplored delivery method for the brain.[18–20] This nonspecific pathway has gained significant attention lately due to observations indicating a transition from clathrin-mediated to caveolae-mediated transcytosis in aging mice.[10] Bacteria[21] and viruses[22] have also been reported to exploit this pathway to cross the BBB. Given that caveolar transport is kept very low at the BBB,[23] studies demonstrate that this pathway is agonist inducible with chemical agents such as methamphetamine or physical stimuli like focused ultrasound.[24,25] These studies imply that heightened caveolar transport for a short duration can open up significant delivery opportunities. It is important to note that caveolae modulators increase overall permeability and might not specifically increase the permeability of the drug or the delivery agent.

To enable the function of nucleic acid cargo, the delivery system must efficiently overcome the poor pharmacokinetics of the nucleic acid.[2] Poly (β-amino ester) (PBAE) systems have shown great potential

Received 2 September 2024; accepted 4 February 2025;
https://doi.org/10.1016/j.omtn.2025.102480.

Correspondence: Munia Ganguli, CSIR-Institute of Genomics and Integrative Biology, Mathura Road, New Delhi 110025, India.
E-mail: mganguli@igib.res.in

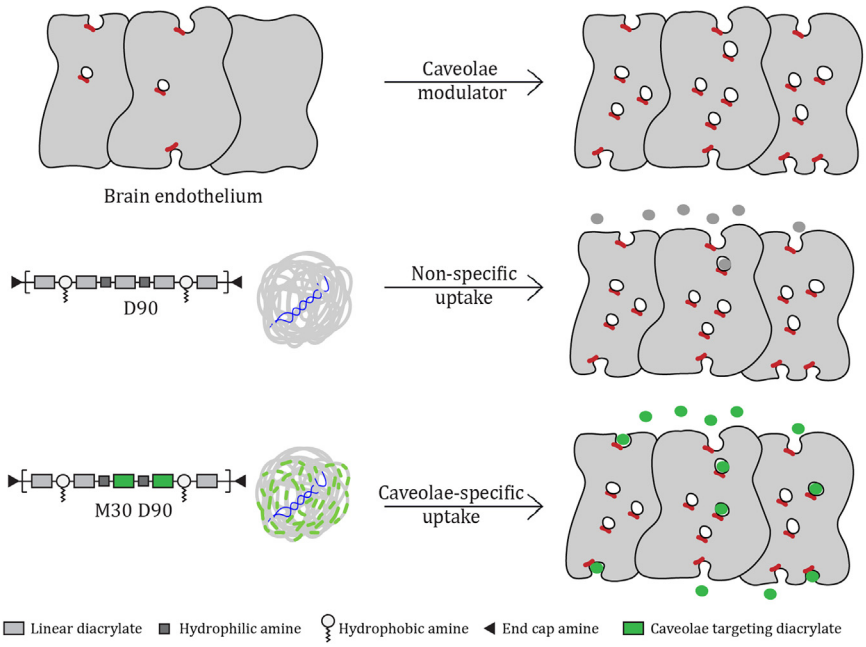

Figure 1. Schematic of the hypothesis suggesting that combining caveolae induction and delivery agent selectively targeting caveolae would help overcome the blood-brain barrier

for nucleic acid delivery. Their chemical versatility is optimized for transfection efficiency and organ targeting.[26–28] While there are no reports of these systems crossing the BBB via systemic routes without additional stimuli like ultrasound,[17] there is evidence of safe and efficient delivery when administered locally.[29–31] These nanoparticle-based delivery systems typically use multiple routes to enter the cell *in vitro*. One way to define nanoparticle selectivity to caveolae-mediated endocytosis is by employing osmotic stimuli.[32] In our previous work, we developed a simple and efficient strategy to synthesize caveolae-selective nanoparticles with PBAE polymers and sugar alcohols.[33] We found that mannitol-modified polymeric nanoparticles retained the osmotic properties of mannitol, enhanced transfection efficiency in neuronal cells, and enabled selective caveolae-mediated endocytosis. We hypothesized that in an *in vivo* scenario, such caveolae-selective nanoparticles in the presence of a caveolae induction model would help nucleic acid delivery across the BBB. Furthermore, we hypothesized that using appropriate monomers for designing the PBAE backbone might avoid delivery to the liver and maximize the chance of reaching the brain.[34]

Our manuscript demonstrates that mannitol-modified nanoparticles (M30 D90) carrying plasmid DNA (pDNA) effectively transfect neuronal cells and enhance transport across brain endothelial cells via the caveolae-mediated transcytosis pathway. We explored the use of systemic hyperosmolar mannitol to induce caveolae at the BBB. Although the direct link between hyperosmolar mannitol administration and increased caveolar transport has not been conclusively proven, speculations suggest this relationship.[35,36] Our findings show that systemic mannitol can induce caveolae in the brain without compromising tight junction integrity or causing neuroinflammation. We show that caveolae abundance is leveraged by M30 D90 enabling improved transfection in the brain *in vivo*. Notably, transfection in the liver was low with M30 D90, and uptake was primarily observed in neurons, highlighting the potential for treating CNS disorders. In summary, we developed and implemented a simple, efficient, and safe polymer-based delivery system for gene delivery to the brain.

RESULTS

Based on literature evidence, we chose to target caveolae-mediated transcytosis for delivery to the brain. We hypothesized that merely inducing caveolae at the BBB would not be sufficient for effective delivery; the cargo delivery system must also exhibit selectivity for caveolae to cross the BBB successfully. To impart selectivity to caveolae-mediated endocytosis, we modified the PBAE polymer with mannitol (Figure 1).

Synthesis and characterization of mannitol-modified nanoparticles

PBAE polymers are synthesized by one-pot Michael's addition of diacrylates and amine monomers. The selection of monomers can affect the efficiency and organ tropism *in vivo*.[37] We chose Bisphenol A ethoxylate diacrylate (D), reported to escape the liver and have better *in vivo* transfection of pDNA (plasmid DNA), over Bisphenol A glycerolate diacrylate (DD), which we have used earlier as the diacrylate monomer.[34] We used 4-(2-aminoethyl) morpholine (S90) and 1-dodecylamine (Sc12) as the two amine monomers for the synthesis of the D90 polymer. For the synthesis of M30 D90, mannitol diacrylate was used to replace D acrylate by 30%, keeping the proportion of the other monomers the same. The exact molar ratios are listed in Table S1. The final polymers of D90 and M30 D90 were obtained by end-capping with diethylenetriamine (E63). The polymer composition and synthesis scheme are depicted in Figure 2A. We confirmed the mannitol substitution in the polymer with proton NMR. We find a 31.8% doping of mannitol in the case of M30 D90, which is close to the theoretical value of 30% used in the reaction (Figures S1 and S2). Gel permeation chromatography (GPC) estimated the molecular weight of D90 to be 5082 Da with a PDI of 1.30 and M30 D90 was 5901 Da with a PDI of 1.14 (Table S2). We further measured the nucleic acid binding and osmolarity of the synthesized polymers. M30 D90 exhibited lower nucleic acid binding compared with D90 (Figure 2B). Additionally, the osmolarity of M30 D90 was higher than that of D90 by about 130 and 230 mOsm for polymer concentrations of 2.5% and 5%, respectively (Figure 2C). M30 D90 also showed a

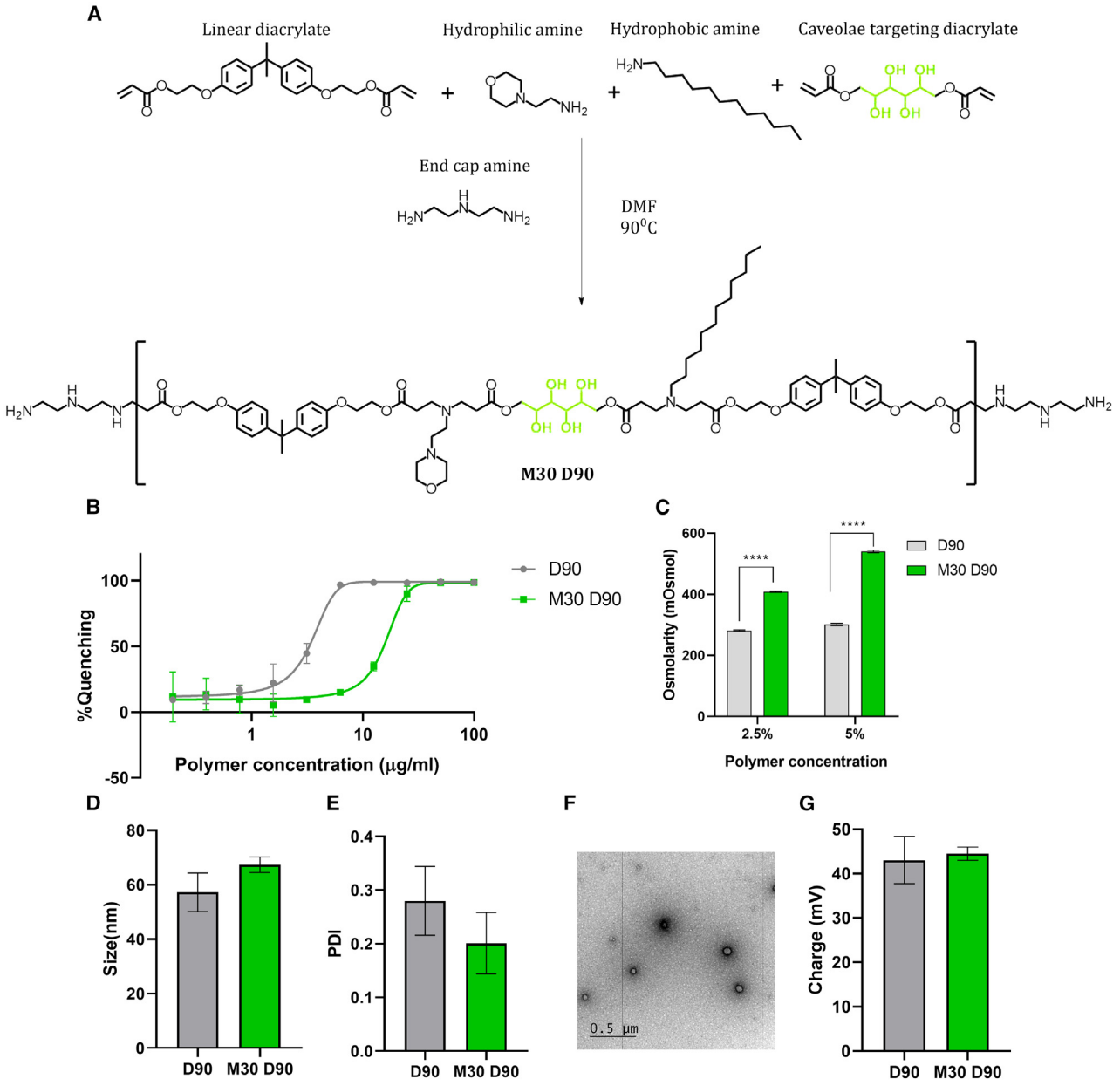

Figure 2. Effects of mannitol modification in D90-Sc12-E63 backbone

(A) Scheme of synthesis of mannitol-modified PBAE. The polymer structure shown is only a representation since the exact sequence is undefined in a statistical copolymer. (B) Polymer and nucleic acid binding studied with RiboGreen assay (C) Osmolality of polymers. Data are shown as mean ± SD, $n = 2$. Significance was calculated by Sidak's multiple comparisons ****$p < 0.0001$. Polymeric nanoparticles were formed with a 1:60 (w/w) ratio of pDNA to polymer in an aqueous buffer. Several nanoparticle properties were measured (D) Hydrodynamic size and (E) Polydispersity Index estimated by dynamic light scattering. (F) Transmission electron micrograph of M30 D90 (Scale: 0.5 μm) and (G) Zeta potential of polymeric nanoparticles. Data represented as mean ± SD, $n = 3$.

concentration-dependent increase in osmolarity while unmodified D90 did not. Analysis using gel electrophoresis revealed complete complexation of pDNA with the polymers at ratios of 1:5 (pDNA to polymer) for D90 and 1:10 for M30 D90 (Figure S3A). This trend is consistent with the nucleic acid binding data, indicating that D90 binds more efficiently, thus completely encapsulating pDNA with less polymer than M30 D90. Release studies with heparin- (as anionic challenge) treated nanoparticles (formed at a 1:60 [w/w] of pDNA to polymer) demonstrated complete release even at low heparin amount (1:0.25 w/w polymer to heparin) in the case of M30 D90. Conversely, while release from D90 nanoparticles initiates at lower amounts of heparin, complete DNA release cannot be achieved even with high

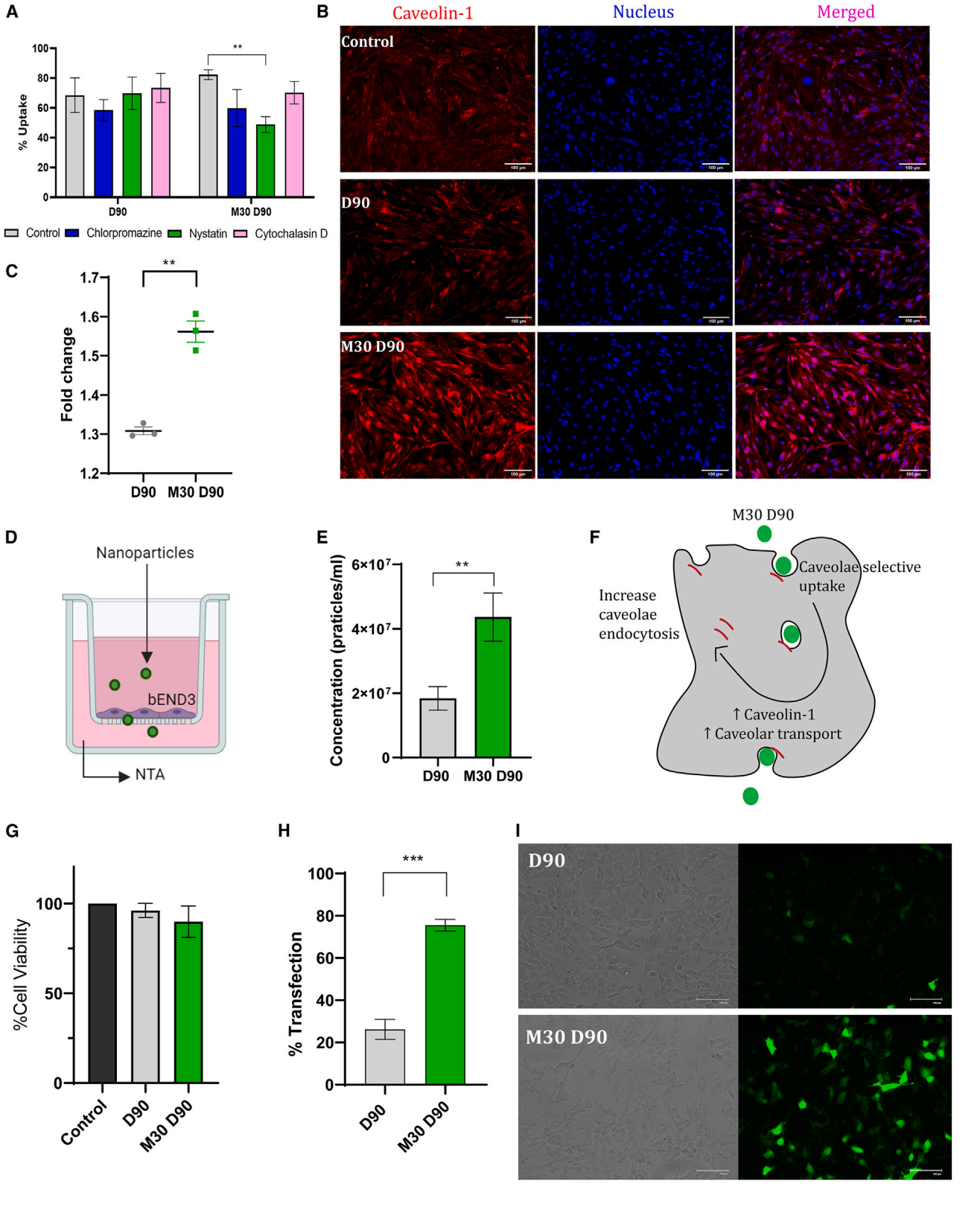

(legend on next page)

heparin ratios (1:32) (Figure S3B). Polymeric nanoparticles were formed via self-assembly in aqueous buffer (25-mM sodium acetate, pH 5.2) by pipette mixing pDNA and the polymer at a 1:60 (w/w) ratio (pDNA:polymer). D90 and M30 D90 polymers formed nanoparticles with pDNA with a hydrodynamic diameter of 60–70 nm (Figure 2D) and polydispersity index less than 0.3 (Figure 2E). Further characterization using transmission electron microscopy (TEM) demonstrated that the morphology was spherical for M30 with pDNA in a ring structure with a hollow center (Figure 2F). The surface charges of D90 and M30 D90 were about +40 mV (Figure 2G). Mannitol modification in D90 did not alter the size and charge of the assembled nanoparticles.

Cellular viability, transfection, and transport of mannitol-modified nanoparticles

Following nanoparticle characterization, M30 D90 was tested for caveolae selectivity in the mouse brain microvascular endothelial cell line (bEND.3) as endothelial cell type would be the first entry point to the brain in an *in vivo* scenario. Cells were pretreated with different endocytosis inhibitors and incubated with labeled nanoparticles (where the pDNA is labeled with ATTO488) followed by flow cytometry to quantify cellular uptake. We observed a significant drop in uptake of about 30% with nystatin (inhibitor of caveolae-mediated endocytosis); however, there was no notable change in uptake with chlorpromazine (inhibitor of clathrin-mediated endocytosis) or cytochalasin D (inhibitor of macropinocytosis) for M30 D90 (Figure 3A). This indicates a significant amount of cellular entry of nanoparticles is through the caveolar route although there could be other pathways that we have not explored here. On the other hand, the uptake of D90 nanoparticles did not drop significantly (and in some cases showed an increase) in the presence of endocytosis inhibitors used in this study, suggesting nonspecific or unexplored modes of uptake. To further validate the involvement of the caveolae-mediated endocytosis pathway, we examined the expression of Caveolin-1 (Cav-1), a primary marker for caveolae. We noted overexpression of Cav-1 at both transcriptional and translational levels with the incubation of M30 D90 (Figures 3B and 3C). To check if selectivity to caveolae-mediated endocytosis led to better penetration, we measured the transport of nanoparticles across the endothelial barrier using an *in vitro* BBB model (Figure 3D). We found a significant increase in the transport of M30 D90 across the endothelial cells compared with D90 (Figure 3E). Our findings collectively demonstrate evidence of caveolar involvement in the uptake and improved transport of the M30 D90 nanoparticles (Figure 3F).

Cellular viability and transfection were assessed in the human neuronal cell line SHSY5Y using reporter plasmid with ubiquitous CMV promoter (pEGFP-C1). M30 D90 and D90 exhibited excellent viability comparable to control, as determined by MTT assay (Figure 3G). Flow cytometry analysis of a low-dose transfection in SHSY5Y cells (300 ng per 24 wells) revealed 80% fluorescence-positive cells M30 D90, whereas D90 showed only about 25% fluorescence-positive cells (Figures 3H and 3I). Additionally, we observed the uptake of M30 D90 was predominantly through caveolae even in the SHSY5Y cell line (Figure S4).

Effect of systemic mannitol administration on caveolae formation in brain endothelial cells

While M30 D90 increases Cav-1 levels in cultured brain endothelial cells, we reasoned that the opportunity for M30 D90 to induce caveolae at the BBB *in vivo* could be limited. In a healthy brain, nonspecific caveolae-mediated endocytosis is kept low.[38] Caveolar transport needs to be induced for nanoparticles to utilize this pathway. Transient upregulation of Cav-1 has been reported to increase the transcytosis rate at the BBB.[39] Previous studies have demonstrated that systemic administration of hyperosmolar mannitol can increase fluid flux and the formation of pinocytic vesicles in the brain.[35,40] There have been speculations that these pinocytic vesicles are caveolae.[36] Earlier reports have noted increased transgene expression with rAAV-mediated delivery followed by systemic mannitol injection.[41,42] Based on this evidence, we administered hyperosmolar mannitol intraperitoneally to induce caveolae formation at the BBB and observed caveolae puncta marked by Cav-1 (Figure 4A). We also confirmed caveolae induction via qRT-PCR, observing a 1.4-fold increase in Cav-1 mRNA levels at 30 min following mannitol administration. Cav-1 mRNA was downregulated at later time points, 6- and 24-h post-injection, suggesting a regulatory mechanism to restore Cav-1 levels and confirming the transient effect of systemic mannitol (Figure 4B). Caveolae induction following mannitol injection is not exclusive to the brain, as we also observed elevated Cav-1 mRNA in the liver and lungs (Figures S5A and S5B). However, since caveolae formation in the brain is extremely low without such a perturbation, the increase in Cav-1 expression within the brain creates a new opportunity for improving the entry of caveolae-targeting nanoparticles to the brain parenchyma.

Figure 3. Effects of mannitol modification on uptake mechanism, transport, and transfection efficiency

(A) Mechanism of endocytosis of nanoparticles (labeled with ATTO488) with pharmacological inhibitors was assessed in mouse brain microvascular endothelial cells (bEND.3). Flow cytometry analysis revealed a drop in uptake of M30 D90 with nystatin (caveolae inhibitor). (B) Immunocytochemistry in brain microvascular endothelial cells (bEND.3) indicating overexpression of Cav-1 protein in M30 D90 following 30-min incubation with nanoparticles (scale bar, 100 μm). (C) qRT of Cav-1 in bEND.3 after 30 min of D90 and M30 D90 treatment (unpaired t test with Welch's correction). (D) Schematic of *in vitro* transwell BBB model. Labeled nanoparticles (ATTO488-labeled plasmid) were added to the apical chamber, and their penetration was assessed by measuring the nanoparticle concentration in media collected from the receptor chamber after 5 h of incubation. (E) Nanoparticle concentration quantified using a Nanoparticle Tracking Analyzer (NTA) shows increased penetration of M30 D90 to D90 (unpaired t test). (F) M30 D90 promotes selective caveolae-mediated uptake, upregulates Cav-1 expression, and enhances transport across endothelial cells. Cell viability and transfection efficiency in a human neuronal cell line (SHSY5Y) with nanoparticles formed with reporter plasmid of green fluorescence protein (pEGFP-C1). (G) Percentage cell viability estimated by MTT assay. (H) Flow cytometry analysis depicting increased percentage transfection with M30 D90 compared with D90 (unpaired t test). (I) Fluorescence microscopy images of transfection (scale bar: 100 μm). Data are presented as mean ± SD, $n = 3$, $^{**}p < 0.01$, $^{***}p < 0.001$.

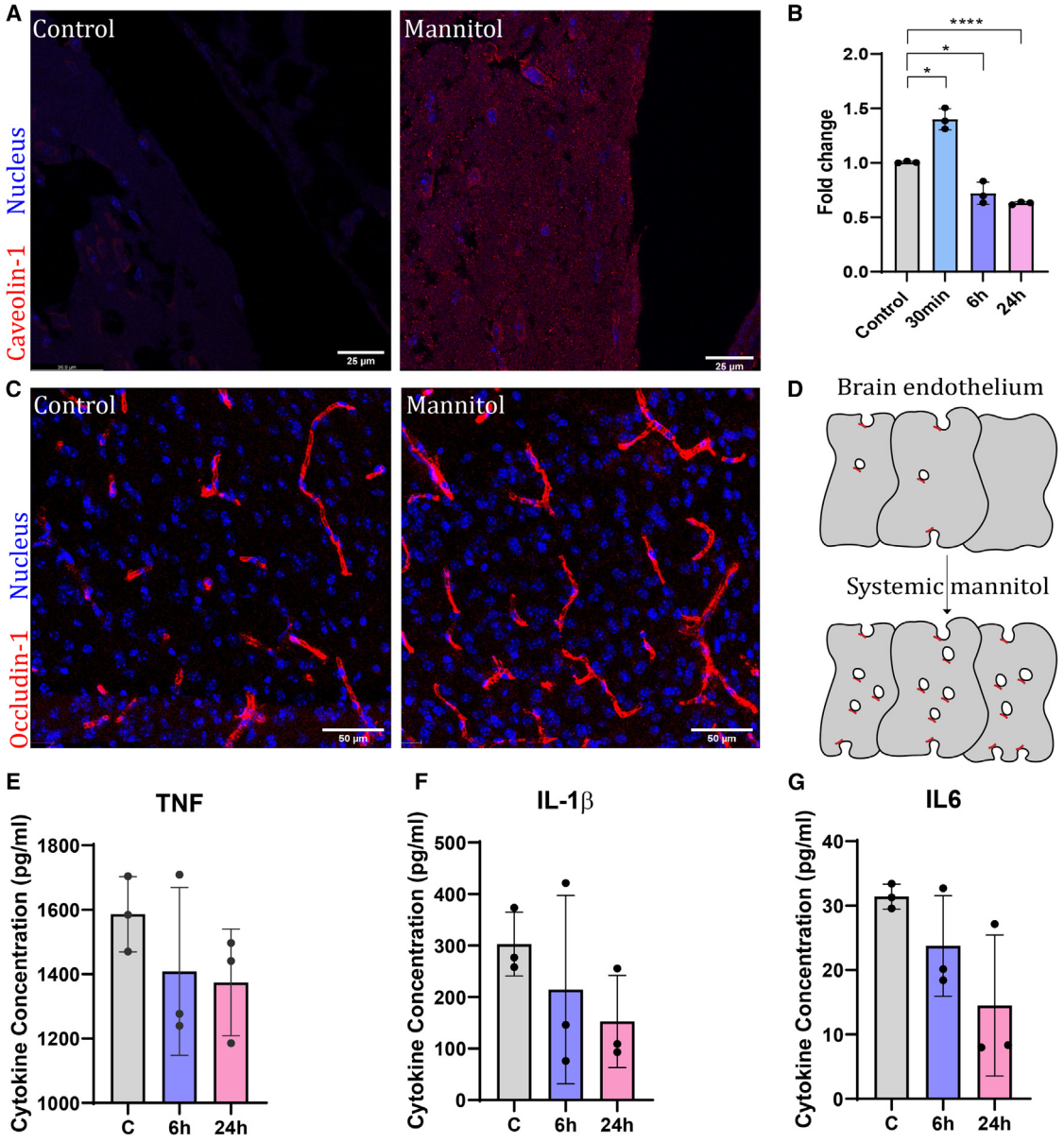

Figure 4. Caveolae can be induced with systemic hyperosmolar mannitol

(A) Immunohistochemistry of Caveolin-1 (Cav-1) expression in the mouse brain 30 min post intraperitoneal injection of mannitol indicates caveolae induction. Representative images depict Cav-1 (red) and nucleus (blue) (scale bar, 25 μm). (B) Cav-1 transcription levels at different time points post mannitol injection depict Cav-1 upregulation at 30 min and downregulation at later time points 6 and 24 h. Significance calculated with t test with Welch's correction. (C) Tight junction integrity post mannitol treatment assessed by tight junction marker Occludin-1 (red) and nuclei (blue) (scale bar, 50 μm). (D) Mannitol induces caveolae in the brain without compromising tight junction integrity. Mannitol injection did not elevate inflammatory markers (E) TNF, (F) IL1-β, and (G) IL-6 in the brain (C-no treatment control). Data represented as mean ± SD, $n = 3$, $^{*}p < 0.1$, $^{****}p < 0.0001$.

To assess the safety of systemic mannitol administration on the brain, we evaluated tight junction integrity by immunostaining for Occludin-1. No significant differences were observed between the control and mannitol-treated groups at the same time point used for caveolae induction analysis (Figure 4C). Systemically administered mannitol appears to enhance intracellular transport by caveolae without disturbing the paracellular transport, as shown schematically in Figure 4D. Systemic mannitol injection did not induce neuroinflammation, as evidenced by the absence of significant changes in tumor necrosis factor (TNF), interleukin (IL)-1β, and IL-6 levels measured at 6- and 24-h post-injection (Figures 4E–4G). Based on these findings, we proceeded to utilize

systemic mannitol administration as an agonist for caveolae induction.

Effect of mannitol-modified polymeric nanoparticles on *in vivo* transfection of the brain

Before proceeding *in vivo*, polyethylene glycol (PEG) was incorporated into the nanoparticle system to enhance stability and reduce interaction with blood components during systemic injection. Alkyl side chains in the polymer backbone allow for the noncovalent incorporation of DMG PEG 2000.[43] Since the PEG association is noncovalent, similar to its use in lipid nanoparticles, where it has been extensively studied, the PEG lipid is expected to eventually dissociate from the nanoparticles while circulating in the blood but also offer improved shielding to the nanoparticles compared with unmodified ones.[44] As a result, PEG is unlikely to hinder nanoparticle interactions with endothelial cells in this format. The percentage of PEG lipid added was optimized and the volume ratio of buffer and ethanol was adjusted to prepare nanoparticles that are smaller than 100 nm as described in the materials and methods section (Figure 5A). D90 and M30 D90 with PEG formed uniform nanoparticles with PDI less than 0.3 (Figure S6A) and sizes less than 100 nm (Figure 5B). TEM analysis reveals the spherical morphology of assembled M30 D90 nanoparticles with DNA localizing in a peripheral ring structure similar to nanoparticles formulated without PEG (Figure 5C). However, there was a significant decrease of over 20 mV in the surface charge, consistent with previous reports (Figure 5D).[27] PEG modification did not alter the *in vitro* transfection trend observed with nanoparticles (Figure S6B). PEG-modified M30 D90 was stable for up to 48 h, as indicated by consistent particle size and PDI measurements taken at regular intervals, demonstrating their stability at room temperature (Figures S6C and S6D).

In vivo transfection efficacy was assessed through *ex vivo* fluorescence imaging. Mice were injected with hyperosmotic mannitol intraperitoneally to induce transient caveolae formation, followed by an intravenous dose of nanoparticles (0.3 mg/kg). After 24 h, organs were harvested, and GFP fluorescence was analyzed using an *in vivo* imaging system (IVIS) (Figure 5E). Mice treated with M30 D90 nanoparticles exhibited relatively strong GFP fluorescence in the brain (Figures 5F and S7A), indicating successful brain transfection. Transfection was also observed in the liver for both D90 and M30 D90 nanoparticles (Figure S7B), while no fluorescence was detected in the lungs or spleen for either formulation (Figures S7C and S7D).

Control experiments with M30 D90 administration and no mannitol pretreatment revealed reduced brain transfection, with GFP expression primarily to the liver and no expression in the lung and spleen (Figure S8). We also noted a decrease in signal in the liver with M30 D90 without pre-mannitol injection, suggesting systemic mannitol may enhance overall transfection due to caveolae induction (Figure 5G). We did not observe transfection at 48 h indicating the transient nature of expression (Figure S9). Since pre-mannitol injection did not result in brain transfection with D90, and without pre-mannitol injection, M30 D90 shows lower transfection in the brain, both mannitol modification and mannitol injection were essential for enhancing delivery to the brain. In such a scenario of coupling the two, approximately 10% of the total signal was from the brain (Figure 5H).

Uptake, localization, and safety profile of M30 D90 nanoparticles after *in vivo* administration

To further confirm the penetration of M30 D90 across the BBB, we checked the brain uptake of M30 D90 nanoparticles formed with ATTO647N-labeled pDNA. Nanoparticles were administered intravenously following intraperitoneal mannitol injection and after 6 h, mouse brains were isolated, fixed, and sectioned for fluorescence imaging. Images captured from the capillary-rich cortex show nanoparticle puncta confirming delivery across the BBB (Figure S10). To examine the uptake of M30 D90 across various cell types, we performed colocalization experiments by immunostaining with cell-type-specific markers for neurons (MAP2), microglia (Iba-1), and astrocytes (GFAP). Our findings revealed colocalization of M30 D90 with neurons, as evidenced by overlapping signals with MAP2 staining (Figure 6A) in the cortex and the hippocampal region (Figure 6B). We did not observe significant colocalization with microglia (Iba-1) or astrocytes (GFAP), suggesting a potential preference for uptake in neurons over other cell types (Figures 6C and 6D).

To investigate the selective uptake of the M30 D90 in neurons, we conducted uptake experiments in two non-neuronal cell lines: astrocytes (C8D1A) and microglia (N9). In astrocytes, the uptake did not exceed 15% with M30 D90 (Figure S11A). While microglia demonstrated a significantly higher uptake, with nearly 98%, there was no drop in the presence of nystatin, suggesting no preference for caveolae-selective endocytosis (Figure S11B). The low uptake and lack of selectivity to caveolae-mediated endocytosis in other cell types could be probable reasons for neuron selectivity observed *in vivo*.

To check the *in vivo* safety profile, we performed liver enzyme assays after 2 and 7 days of a single injection of M30 D90 with pre-mannitol injection. No significant difference was noted in the levels of alanine transaminase (ALT) and aspartate transaminase (AST) (Figure S12A) between the control and M30 D90, confirming no hepatotoxicity. Next, we assessed brain histology 1 day after M30 D90 nanoparticle exposure. No necrosis or inflammation was observed with H&E-stained brain sections (Figure S12B).

DISCUSSION

Most strategies for brain delivery focus on increasing nanoparticle transcytosis with receptor-ligand engagement. Despite success with the delivery of antibodies and oligonucleotides,[45,46] these strategies could not be adopted effectively for nanoparticle systems carrying macromolecular cargoes like plasmids. The observation of a physiological shift from clathrin- to caveolae-mediated transcytosis at the BBB in aged conditions and certain diseased states indicates that caveolae-mediated transcytosis can be an alternative route to overcome BBB.[10,19] Strategies that modulate caveolae-mediated transcytosis directly or indirectly at the BBB are emerging.[24,25,47,48] Since caveolae

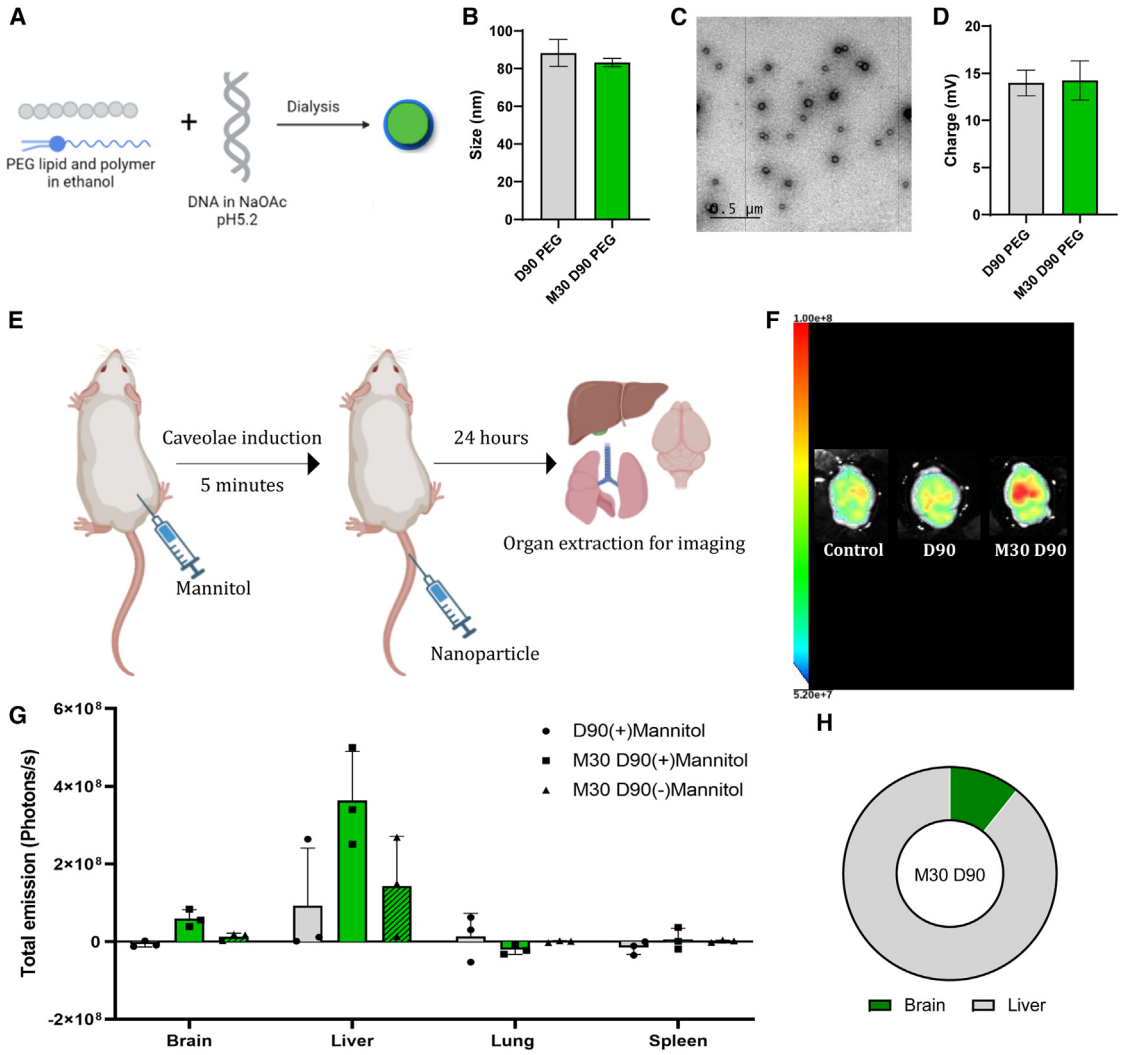

Figure 5. PEG-incorporated M30 D90 transfects the brain following caveolae induction

(A) Scheme of PEG lipid incorporation in polymeric nanoparticles. (B) Hydrodynamic size of PEG-incorporated nanoparticles. (C) Transmission electron micrographs depicting spherical morphology. (D) Surface charge of nanoparticles after incorporation. (E) Nanoparticle administration scheme following pre-injection of hyperosmotic mannitol for caveolae induction. (F) Representative vivo imaging system (IVIS) image of GFP expression in the brain. Transfection was measured in three conditions: caveolae induction followed by D90 injection (D90 (+) Mannitol), caveolae induction followed by M30 D90 injection (M30 D90 (+) Mannitol), and just M30 D90 injection (M30 (–) Mannitol). Relative fluorescence as total emission was calculated by subtracting control fluorescence from treated groups. (G) Fluorescence from the brain and other peripheral organs—liver, lung, and spleen. (H) GFP expression plotted as the percentage total emission from the brain and liver calculated from *ex vivo* IVIS fluorescence images of M30 D90 with caveolae induction. Data reported as mean +SD with n = 3 biological replicates.

are actively suppressed in the brain by lipid transporter major facilitator superfamily domain containing 2a (Mfsd2a),[23] transient upregulation of caveolae-mediated transcytosis at the BBB has enabled the transport of small and large cargoes to the brain. In our current work, we emphasize the need for nanoparticle selectivity toward caveolae-mediated endocytosis to exploit the permeability advantage created by caveolae enhancers.

Our initial experiments centered on developing nanoparticles that target caveolae-mediated endocytosis for cellular entry. To achieve caveolae selectivity for the delivery agent, sugar alcohols have been reported that enable an osmotic environment on the cell membrane and drive caveolae endocytosis by rapidly phosphorylating Cav-1.[32] For the delivery system, we selected PBAE due to its modular structure, ease of chemical modification, and established effectiveness in nucleic acid delivery. They are actively pursued for nucleic acid delivery and have shown immense potential in preclinical models with mRNA vaccines, and cancer therapies.[26,49] Caveolae selectivity in PBAE was introduced by substituting mannitol as one of the monomers making it a part of the polymer in the

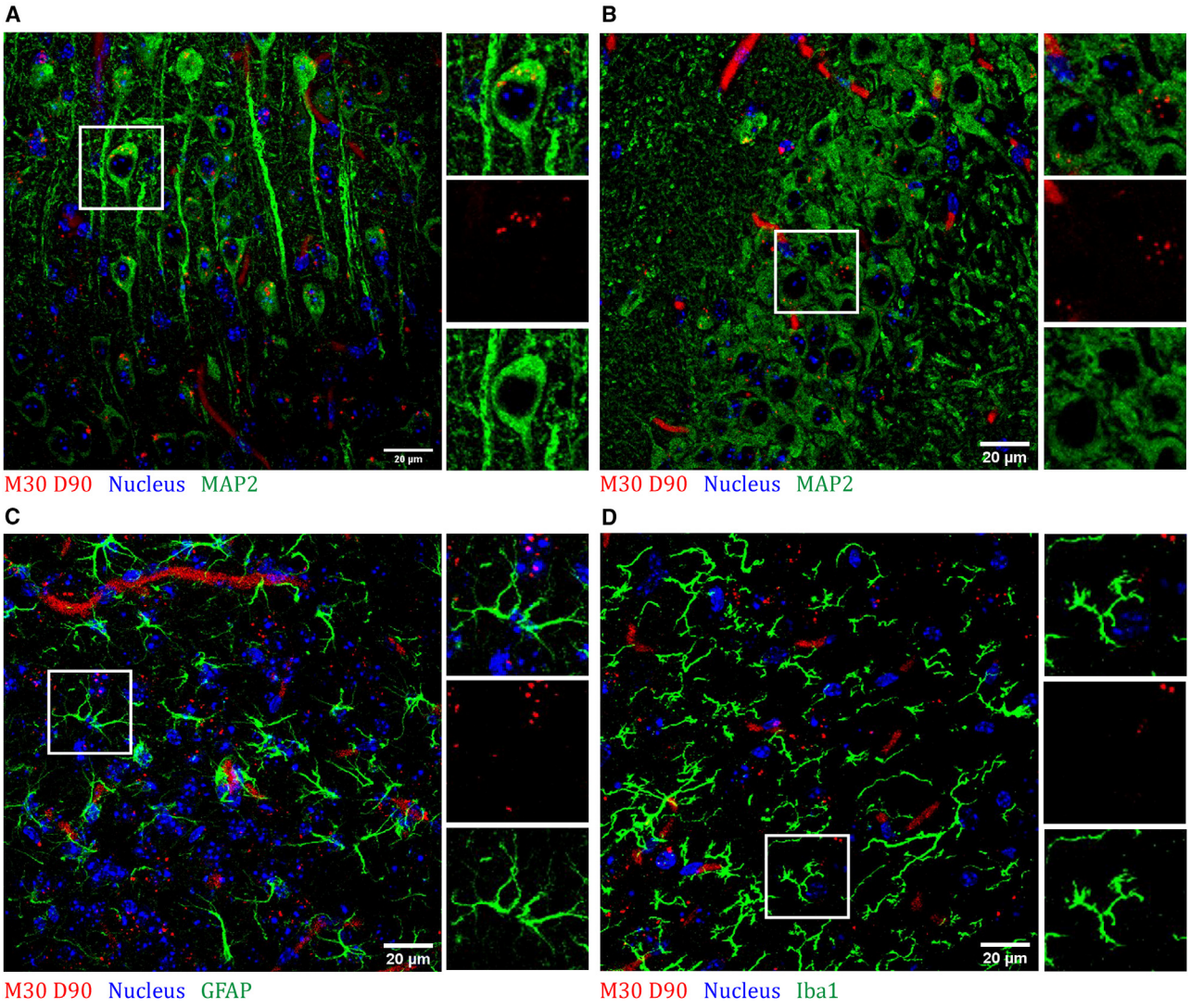

Figure 6. M30 D90 uptake is selective to neurons in the brain *in vivo*

The biodistribution of M30 D90 *in vivo* was analyzed by intravenous administration of ATT0647N-labeled pDNA following caveolae induction ($n = 3$). Immunohistochemistry with neuron marker MAP-2 (green) indicates colocalization of M30 D90 nanoparticles (red), (A) in the cortex, and (B) in the hippocampus. Nanoparticle colocalization was not observed with (C) microglia (Iba-1, green), or (D) astrocytes (GFAP, green). Z-stacked images depict cell markers (green), nanoparticles (red), and nuclei (blue). Scale bar, 20 μm.

synthesis step. Recent studies have highlighted the potential for ligand-free organ selectivity, demonstrating that even minor structural modifications, whether through complete or partial substitutions, can profoundly influence the tropism of delivery systems.[34,50,51] Such a system is highly advantageous due to its simplicity, scalability, and cost-effectiveness. To redirect nanoparticles predominantly accumulating in the liver to other organs, we swapped the diacrylate from bisphenol A glycerolate (DD) used in our earlier work to bisphenol A ethoxylate diacrylate (D).[34] We observed that mannitol modification in the D90-Sc12-E63 backbone (M30 D90) retained the osmotic property of mannitol and nucleic acid binding ability to form nanoparticles below 100 nm M30 D90 shows selectivity to caveolae-mediated endocytosis as confirmed with pharmacological inhibitors and increased Cav-1 levels in brain microvascular endothelial cells. The caveolae selectivity also translated to better caveolae-mediated transcytosis across the endothelium assayed by the transwell system predicting better delivery. The transfection efficiency in neuronal cell line (SHSY5Y) of M30 D90 is 3-fold higher than D90, which could be explained by the complete release of pDNA as observed with heparin. Efficient complexation accompanied by efficient release has been a good predictor of transfection efficiency.[52] In addition, selectivity to caveolae-mediated endocytosis is an enabler of transfection efficiency because caveolae have a non-degradative fate in the cell.[53]

Our second set of experiments aimed to create a transient caveolae-abundant state at the BBB to facilitate the entry of caveolae-selective nanoparticles. To achieve this, we investigated the potential of systemic mannitol as an agonist for caveolae induction. Depending on the administration route, mannitol can transiently enhance paracellular or intracellular transport. When administered via intracarotid injection, mannitol has been shown to temporarily disrupt the BBB by opening tight junctions in the brain.[36] In contrast, systemic mannitol administration has been associated with increased fluid flux in the brain, a process believed to be mediated by caveolae.[40] Our findings demonstrate that systemic hyperosmolar mannitol increases caveolae levels, confirmed by immunostaining and transcriptional upregulation of Cav-1. At later time points (6 and 24 h), Cav-1 expression is downregulated, indicating the transient nature of this effect. Systemic mannitol injection preserves paracellular permeability, as evidenced by intact tight junctions marked by Occludin-1 expression. However, it subtly alters vascular architecture, with vasodilation observed as an increase in vessel diameter in immunostaining images. Moreover, mannitol administration is safe, showing no indications of neuroinflammation. Thus, systemic mannitol injection serves as a safe and effective model for global caveolae induction in the brain. However, caveolae induction through systemic mannitol is not brain-specific; it also elevates Cav-1 mRNA levels in peripheral organs, including the lungs and liver. While this lack of brain exclusivity could be a limitation, systemic mannitol offers the advantage of broad CNS distribution, which may be beneficial depending on the therapeutic requirements.

In our subsequent experiments, we combined caveolae induction with caveolae-selective nanoparticles to achieve efficient brain delivery. PEG-incorporated M30 D90 crossed the BBB to transfect the brain following caveolae induction with hyperosmolar mannitol at a clinically relevant dose. Without caveolae induction, caveolae-selective nanoparticles (M30 D90) exhibited lower brain transfection. Conversely, even with caveolae induction, non-caveolae-selective nanoparticles (D90) failed to achieve brain transfection. To validate the caveolae induction and targeting strategy, we also tested M30 DD90 (mannitol-modified on the DD90-Sc-12 backbone), as reported previously. Our results showed that M30 DD90 achieved brain transfection with caveolae induction. However, the transfection levels in the brain and the brain-to-liver ratio were lower compared with those observed with M30 D90 (data not shown). These results strongly indicate that the mannitol modification needs to be coupled with appropriate monomer composition and combined with pre-mannitol injection to achieve efficient transfection in the brain. We observed that M30 D90 was distributed throughout the brain, with predominant uptake in neurons, highlighting its potential for targeted, cell-type-specific applications. The uptake in astrocytes was low and in the case of microglia, selectivity to caveolae-mediated endocytosis was not observed. Microglial uptake discrepancies between *in vitro* and *in vivo* models may stem from the culture environment, which can induce stress and activate microglia, potentially increasing uptake *in vitro*.[54,55] The specificity to the neurons could therefore be because of the strong caveolae-mediated uptake. Further exploration into the monomer composition might enable us to understand cell-type specificity better.

A key limitation of our caveolae induction model with systemic mannitol is the relative lack of specificity, as it also affects other organs. In brain-targeted therapies, precise delivery is often crucial.[56] Selective caveolae induction in the brain might be challenging with systemically administered agonists although the level of induction would certainly be improved in the presence of such a systemic administration of an osmotic agent like mannitol. In the future, low-dose focused ultrasound (FUS) can be coupled to our nanoparticles as a promising approach to achieve region-specific caveolae induction within the brain. Targeted FUS could enable localized access of the caveolae-targeting nanoparticles to specific brain areas allowing for greater precision in delivering therapeutics. To add another layer of specificity, payload optimization with neuron-specific promoters like Syn-1 can be utilized.[57]

In summary, this study highlights the role of caveolae-mediated transcytosis as a strategy in the development of delivery agents for the brain. We strategically designed a nanoparticle system based on PBAE polymer modified with mannitol to target the caveolae-mediated endocytosis pathway for crossing the BBB. We also used systemic mannitol injection to enhance caveolae formation at the BBB and facilitate the entry of these nanoparticles. We establish that this combination can significantly enhance delivery to the brain. This work provides the foundation for exploring systems based on caveolae-mediated transcytosis for nucleic acid delivery to the brain.

MATERIALS AND METHODS

Bisphenol A ethoxylate diacrylate (413550), 4-(2-aminoethyl) morpholine (S90; CAS 2038-031), 1-Dodecylamine (Sc12; CAS 124-22-1), Diethylenetriamine (E63; CAS 111400), Mannitol (CAS 69658), Pyridine (CAS 110861), Chlorpromazine Hydrochloride (C0982), Nystatin (N9150), Cytochalasin D (C8273), ATTO488 amine (74417), ATTO647N amine (95349), SPB (succinimidyl-[4-(psoralen-8-yloxy)] butyrate) (803545), DMSO-D6, Dimethylformamide (CAS 68-12-2), Diethyl ether (CAS 60-29-7), Thiazolyl Blue Tetrazolium Bromide (M5655), DMG PEG 2000 (880151P-1G), Spectra-Por Float-A-Lyser G2 (Z726710-12EA), ALT activity assay (MAK052), AST activity assay (MAK055) were purchased from Sigma-Aldrich. Acryloyl chloride (CAS 2123990) was purchased from Alfa Aesar. The pEGFP-C1 plasmid (4.7 kb) was amplified in *Escherichia coli* DH-5α and pDNA isolated with GenEluteTM (Sigma-Aldrich). The primary antibody against Caveolin-1 (ab2910), GFAP (ab7260), MAP-2 (ab32454), and Iba-1 (ab178846) was purchased from Abcam. Occludin (3E11.11) was procured from DSHB. Secondary antibodies Alexa Fluor 594 goat anti-rabbit (A11012), Alexa Fluor 488 goat anti-rabbit (A11008), Alexa Fluor 568 goat anti-rat (A11077), and Prolong Gold AntiFade with DAPI (P3693) were procured from Thermo Fisher Scientific. Costar 6.5-mm transwell permeable support with 3-μm pore polyester membrane (3472) was procured from Corning.

Mannitol-modified polymer synthesis and characterization

The polymers were synthesized as previously reported.[33] Briefly, diacrylate - Bisphenol A ethoxylate diacrylate (D), hydrophilic amine - 4-(2-aminoethyl) morpholine (S90), and hydrophobic amine - (1-Dodecylamine) (Sc-12) were reacted for 24 h in DMF to synthesize the base polymer of D90. For mannitol modification, we first synthesized the mannitol diacrylate monomer by reacting 2 mol of acryloyl chloride to 1 g of mannitol in 20 mL of DMF and 10 mL of pyridine for 24 h at 4°C. Mannitol diacrylate was precipitated and purified with diethyl ether and dried. Mannitol diacrylate was substituted at a 30% molar ratio to Bisphenol A ethoxylate diacrylate to form M30 D90. Both the polymers were capped with Diethylenetriamine (E63) in THF for 2 h to get the final polymers. Polymers were purified with diethyl ether and vacuum-dried. Polymers were characterized with 400 MHz Bruker (400 MHz for 1H-NMR) to confirm mannitol incorporation in the backbone. The molecular weight of the polymers was evaluated with GPC (Malvern Omnisec instrument having an RI detector and Shodex KD-806 M). The polymers were dissolved in anhydrous DMSO and stored at −20°C until further use.

Nucleic acid binding assay

Polymers were evaluated for nucleic acid binding with RiboGreen. D90 and M30 D90 polymers were serially diluted from 100 μg/mL concentration in 25 mM sodium acetate buffer. The pDNA (pEGFP-C1) solution was prepared at a 1 μg/mL stock concentration with RiboGreen dye in 25 mM sodium acetate buffer. Twenty-five microliters of the polymer solution was mixed with 75 μL of nucleic acid/RiboGreen solution in 96 well-black bottom plates. The samples were incubated for 20 min at 37°C and fluorescent reading was taken in Tecan multi-plate reader excited at 490 nm the fluorescence emission intensity was measured at 530 nm. The quenching percentage was calculated using the formula: (fluorescence of free DNA − fluorescence of polymer-bound DNA)/fluorescence of free DNA) × 100. Half maximal inhibitory concentration (IC50) value was obtained by plotting the fluorescence quenching as a function of polymer concentration and fitting a sigmoid curve to the data. Lower IC50 values indicate higher binding and vice versa.

Osmolarity measurement

The osmolarity of the polymers was measured at 2.5% and 5% of polymer concentration in 100 mM sodium acetate buffer at pH 5.2. Reading was measured using a cryoscopic osmometer (OSMOMAT 3000 Microprocessor).

Nanoparticle formation and characterization

Nanoparticles were formed by pipette mixing pDNA and polymer at 1:60 (w/w) in 25 mM sodium acetate (pH 5.2). Nanoparticles were diluted in MilliQ for size and 10 mM NaCl for zeta measurement at a concentration of 0.002 μg/μL. Measurements were taken with Zetasizer Nano ZS (Malvern Instruments, UK).

Gel electrophoresis

Complexation and release studies were done using agarose gel electrophoresis. Agarose gels were cast with 1% agarose dissolved in Tris-Acetate-EDTA buffer. Twenty-five nanograms of pDNA was loaded per well. To pDNA, different w/w ratios of polymer were added (1:0.5, 1:1, 1:5, 1:10, 1:201:30, 1:40, 1:60). For release studies, the pDNA to polymer ratio was fixed to a 1:60 (w/w) ratio and the heparin weights were set in gradients 1:0.25, 1:0.5, 1:1, 1:2,1:4, 1:8, 1:16, and 1:36 to the polymers. Orange loading dye was added to the sample before loading the sample to the gel, electrophoresis was run at 100 V for 10 min, and the gel was visualized using gel doc.

Transmission electron microscopy

TEM imaging was conducted to gain insight into the structure and localization of DNA within the nanoparticle. Assembled nanoparticles were placed onto 200-mesh copper grids. Subsequently, the copper grids were washed using ultrapure water to eliminate buffer salts. Afterward, the grids were rinsed with 1% uranyl acetate in ultrapure water and air-dried overnight. The samples were then analyzed using the TECNAI G2 20 Twin electron microscope, capturing 10–15 fields for each sample.

Cell culture

SHSY5Y cell line (human neuroblastoma) was provided by Dr. Beena Pillai at CSIR-IGIB. N9 (mouse microglia) and C8D1A (mouse astrocytes) were kindly provided by Dr. Anirban Basu at NBRC. bEND.3 cell line (mouse brain microvascular endothelium) was procured from AddexBio. N9 was cultured in RPMI media supplemented with 10% fetal bovine serum (FBS). SHSY5Y, C8D1A, bEND.3, and N2a cells were cultured in Dulbecco's modified Eagle's medium supplemented with 10% FBS. Media and FBS were procured from Gibco and standard cell culture conditions were followed.

Plasmid labeling

Plasmid DNA was labeled with ATTO488 and ATTO647N as reported earlier.[58] One hundred microliters (1 μg/μL) of pDNA was incubated with 12.5 μL (1 μg/μL) of NHS psoralen in a round-bottom 96-well plate for crosslinking under a 365-nm UV lamp for 25 min. Following the crosslinking reaction, ATTO488 or ATTO647N amine was added and incubated for 1 h at room temperature. The labeled plasmid was purified by ethanol precipitation. pDNA was resuspended in nuclease-free water and stored at −20°C for further use.

Mechanism of endocytosis

The mechanism of endocytosis was assayed in bEND.3, SHSY5Y, N9, and C8D1A cell lines. Cells were seeded at a density of 75,000 cells per 24-well plate. Confluent wells were treated with endocytosis inhibitors at the following concentrations: Chlorpromazine (10 μg/mL), Cytochalasin D (500 nM), and Nystatin (50 μg/mL). Following 1 h of incubation with the inhibitors, nanoparticles of D90, and M30 D90 prepared with ATTO488 labeled pDNA were added at a dose of 300 ng per 24-well plate, and the cells were processed for flow cytometry after 2 h. Data were collected on a BD Accuri C6 flow cytometer and analyzed using BD Accuri C6 software.

Immunocytochemistry in bEND.3

bEND.3 cells were seeded onto coverslips in a six-well plate, at a density of 100,000 cells per well, allowing them to adhere overnight. Cells

were incubated with nanoparticles formed with 2 μg pDNA per well for 30 min and were subsequently fixed using 4% paraformaldehyde for 15 min at room temperature. Following fixation, cells were permeabilized using a permeabilization buffer (0.1% Triton X-100 in PBS) for 5 min. After that, the cells were immersed in a blocking buffer (5% BSA in PBS with 0.1% Tween 20) for 1 h at room temperature. The primary antibody (anti-Caveolin-1 antibody), at 1:500 dilution buffer, was added to the blocking buffer and left overnight at 4°C in a humid chamber. Coverslips were washed with wash buffer (0.1% Tween 20 in PBS) and secondary antibody (goat anti-rabbit secondary antibody Alexa Fluor 594), diluted 1:800 in the blocking buffer, was added to the coverslip, and incubated for 1 h. After washing the coverslips three times with wash buffer, the coverslips were mounted with Prolong antifade with DAPI (Life Technologies). The images were taken with the Life Technologies Floid Cell Imaging Station.

qRT-PCR

Following 30 min of nanoparticle treatment, total messenger RNA was isolated from bEND.3 cells/tissue lysate using trizol method with TRI Reagent. Following reverse transcription with the iScript cDNA synthesis kit (Bio-Rad), the transcripts were quantified using KAPA SYBR FAST according to the manufacturer's instructions in the PCR instrument (Bio-Rad). Fold changes in expression were calculated using the ΔΔCT method. The GAPDH gene was used to normalize results. The primer sequences were taken from the previous report and are listed in Table S3.[20]

Penetration assay

bEnd.3 cells were seeded on the upper surface of the membrane in polyester transwell inserts (3 μm pore size, and 6.5 mm diameter) at a density of 25,000 cells per well. Media were changed every other day. Cells were cultured for 5–7 days until a confluent monolayer was formed. Nanoparticles formed with ATTO488-labeled plasmid (at a dose of 500 ng) were added to the upper chamber in flurobrite media containing FBS. The penetration of nanoparticles across the cells was assessed by measuring the nanoparticle concentration from the basal well media after 5 h of incubation. Nanoparticle concentration was determined by Nanoparticle Tracking Analyzer (NTA) (NanoSight NS300), samples were loaded on the top plate and analyzed through a long pass filter with a wavelength cutoff of 500 nm to identify the nanoparticles. For each sample, 5 × 60-s videos were recorded at 25°C and the concentrations were obtained using NanoSight software.

Transfection and cytotoxicity

SHSY5Y cells were seeded at 50,000 cells per well in 24-well plates. Nanoparticles formed with GFP reporter plasmid were treated to the cells in complete media for 24 h, with 300 ng pDNA per 24-well plate. After 24 h, cytotoxicity was estimated by MTT assay, and transfection efficiency was measured through flow cytometry. Fluorescence images of transfection were taken using the Life Technologies Floid Cell Imaging Station.

Nanoparticle assembly for *in vivo* delivery

PEG lipid was introduced in the nanoparticle system to enable systemic stability in serum for *in vivo* delivery. Nanoparticles were formulated with a 1:60 w/w ratio. PEG lipid (10% by weight of polymer) and polymer in absolute ethanol were mixed with pDNA in sodium acetate buffer (pH 5.2). The pDNA and polymer-PEG lipid solution was mixed by pipetting at a 3:1 volume ratio and incubated for 10 min at room temperature for nanoparticle formation. The nanoparticles were dialyzed for 2 h with a 20 kDa Float-A-Lyser G2 dialysis device against PBS at 4°C.

Animal studies

The Institutional Animal Ethics Committee approved all animal procedures. All experiments were performed on 6- to 8-week-old BALB/C female mice.

Caveolae induction

For caveolae induction, 20% mannitol solution prepared in saline was injected intraperitoneally (0.8M mannitol). To check the effect of systemic mannitol in caveolar transport, the mouse brain was collected after 30 min and 6 and 24 h. Brain tissue after 30 min of mannitol treatment was fixed in 4% (w/v) PFA overnight at 4°C before preservation in 30% (w/v) sucrose in PBS. The brain was embedded in OCT compound (Leica) and sectioned at a thickness of 15 μm on a freezing–sliding microtome. Sections were blocked with 5% horse serum and 1% bovine serum albumin followed by the addition of primary antibodies (Caveolin-1 and Occludin-1) for overnight incubation at 4°C. After washing steps, secondary antibodies were added according to the manufacturer's dilution. The tissue samples were sealed with a coverslip with antifade mountant containing DAPI. Images were acquired using Leica SP8 confocal microscope. The length of caveolae induction was monitored by Cav-1 mRNA levels estimated by qRT-PCR at 30 min and 6 and 24 h. Caveolae induction in other peripheral organs (liver and lungs) were quantified with qRT-PCR at 30 min post mannitol injection.

In vivo cytokine measurements

To ensure the safety of intraperitonially administered mannitol, cytokine levels were quantified in serum and brain tissue lysates following mannitol treatment using BD Biosciences ELISA kits. Mice treated with hyperosmolar mannitol to induce caveolae formation were euthanized at 6- and 24 h post-treatment. Serum and brain lysate samples were assessed for proinflammatory cytokines TNF (555268), IL-1β (559603), and IL-6 (555240) according to the manufacturer's instructions. Serum cytokine levels could not be detected with these kits. Hence, only the cytokine levels measured from brain samples are discussed in the results.

In vivo transfection

In vivo transfection was checked with GFP reporter plasmid (pEGFP-C1) with and without caveolae induction with pre-mannitol injection. For nanoparticles administered with caveolae induction, hyperosmolar mannitol was injected intraperitoneally. After 5 min of mannitol injection, PEG-incorporated nanoparticles encapsulating reporter

plasmid were injected via the lateral tail vein at a 0.3 mg/kg dose. After 24/48 h, animals were euthanized via thiopental injection, and selected organs were extracted for imaging with IVIS (Spectral Instruments Imaging System Lago X). For transfection without caveolae induction, only M30 D90 was administered intravenously and organ fluorescence was measured with IVIS after 24/48 h.

In vivo uptake

M30 D90 uptake in the brain was checked with nanoparticles formed with ATTO647N-labeled plasmid. Following caveolae induction with hyperosmolar mannitol, labeled M30 D90 nanoparticles were administered intravenously at a dose of 0.3 mg/kg. After 6 h, the brain was isolated, fixed, and sectioned for immunostaining. Sections were blocked with 5% horse serum before incubation at 4°C with primary antibodies MAP2 (neuronal marker), GFAP (astrocyte marker), or Iba-1 (microglial marker) (dilutions were as per manufacturer's protocol). Sections were washed, stained with Alexa Fluor-conjugated secondary antibodies, and mounted with antifade and coverslip before imaging on a Leica SP8 confocal microscope.

In vivo safety

For *in vivo* safety profiling, blood was collected 2 and 7 days after nanoparticle administration. Blood was centrifuged at 13,000 rpm for 10 min to retrieve serum. Liver enzyme assays AST and ALT activity were measured according to manufacturers' protocol (Sigma-Aldrich, St. Louis, MO). Brain sections were stained for H&E and imaged on Nikon digital sight DS-U3 under 4× magnification.

Statistics

Statistical analyses were performed using GraphPad Prism software (GraphPad Software, Inc).

DATA AND CODE AVAILABILITY

The data presented in this study are available on request from the corresponding authors.

ACKNOWLEDGMENTS

We thank the Council of Scientific and Industrial Research (MLP2011) for the financial support to carry out the work. CSIR-GATE supports B.R.G. for the fellowship. We thank Dr. Beena Pillai at CSIR-IGIB and Dr. Avinash Bajaj and Somesh Jha (RCB) for their valuable experimental insights and support. We thank Koushika (CSIR-IGIB) for helping with confocal and the National Institute of Immunology for the technical support with TEM, tissue sectioning, and H&E staining. We thank Dr. Anirban Basu at NBRC and Dr. Beena Pillai at CSIR for providing the cell lines used in this study. Figures were created with Adobe Illustrator and BioRender.

AUTHOR CONTRIBUTIONS

B.R.G.: Conceptualization, methodology, formal analysis, investigation, visualization, writing – original draft preparation, writing – review & editing. C.M.: Formal analysis. A.K.: investigation. M.P.: Investigation. V.C.C.: Formal analysis. S.G.: Project administration, supervision, writing – review & editing. A.P.: Project administration, supervision, writing – review & editing. M.G.: Conceptualization, funding acquisition, investigation, project administration, supervision, writing – review & editing.

DECLARATION OF INTERESTS

The authors declare no competing interests.

SUPPLEMENTAL INFORMATION

Supplemental information can be found online at https://doi.org/10.1016/j.omtn.2025.102480.

REFERENCES

1. Zheng, M., Tao, W., Zou, Y., Farokhzad, O.C., and Shi, B. (2018). Nanotechnology-Based Strategies for siRNA Brain Delivery for Disease Therapy. Trends Biotechnol. *36*, 562–575. https://doi.org/10.1016/j.tibtech.2018.01.006.

2. Lu, Z.G., Shen, J., Yang, J., Wang, J.W., Zhao, R.C., Zhang, T.L., Guo, J., and Zhang, X. (2023). Nucleic acid drug vectors for diagnosis and treatment of brain diseases. Signal Transduct. Target. Ther. *8*, 39. https://doi.org/10.1038/s41392-022-01298-z.

3. Chow, B.W., and Gu, C. (2015). The Molecular Constituents of the Blood-Brain Barrier. Trends Neurosci. *38*, 598–608. https://doi.org/10.1016/j.tins.2015.08.003.

4. Banks, W.A. (2016). From blood-brain barrier to blood-brain interface: New opportunities for CNS drug delivery. Nat. Rev. Drug Discov. *15*, 275–292. https://doi.org/10.1038/nrd.2015.21.

5. Terstappen, G.C., Meyer, A.H., Bell, R.D., and Zhang, W. (2021). Strategies for delivering therapeutics across the blood–brain barrier. Nat. Rev. Drug Discov. *20*, 362–383. https://doi.org/10.1038/s41573-021-00139-y.

6. Sela, M., Poley, M., Mora-Raimundo, P., Kagan, S., Avital, A., Kaduri, M., Chen, G., Adir, O., Rozencweig, A., Weiss, Y., et al. (2023). Brain-Targeted Liposomes Loaded with Monoclonal Antibodies Reduce Alpha-Synuclein Aggregation and Improve Behavioral Symptoms in Parkinson's Disease. Adv. Mater. *35*, e2304654. https://doi.org/10.1002/adma.202304654.

7. Wyatt, E.A., and Davis, M.E. (2020). Nanoparticles Containing a Combination of a Drug and an Antibody for the Treatment of Breast Cancer Brain Metastases. Mol. Pharm. *17*, 717–721. https://doi.org/10.1021/acs.molpharmaceut.9b01167.

8. Oikari, L.E., Pandit, R., Stewart, R., Cuní-López, C., Quek, H., Sutharsan, R., Rantanen, L.M., Oksanen, M., Lehtonen, S., de Boer, C.M., et al. (2020). Altered Brain Endothelial Cell Phenotype from a Familial Alzheimer Mutation and Its Potential Implications for Amyloid Clearance and Drug Delivery. Stem Cell Rep. *14*, 924–939. https://doi.org/10.1016/j.stemcr.2020.03.011.

9. Tracy, G.C., Huang, K.Y., Hong, Y.T., Ding, S., Noblet, H.A., Lim, K.H., Kim, E.C., Chung, H.J., and Kong, H. (2023). Intracerebral Nanoparticle Transport Facilitated by Alzheimer Pathology and Age. Nano Lett. *23*, 10971–10982. https://doi.org/10.1021/acs.nanolett.3c03222.

10. Yang, A.C., Stevens, M.Y., Chen, M.B., Lee, D.P., Stähli, D., Gate, D., Contrepois, K., Chen, W., Iram, T., Zhang, L., et al. (2020). Physiological blood–brain transport is impaired with age by a shift in transcytosis. Nature *583*, 425–430. https://doi.org/10.1038/s41586-020-2453-z.

11. Tachibana, K., Hashimoto, Y., Shirakura, K., Okada, Y., Hirayama, R., Iwashita, Y., Nishino, I., Ago, Y., Takeda, H., Kuniyasu, H., and Kondoh, M. (2021). Safety and efficacy of an anti-claudin-5 monoclonal antibody to increase blood–brain barrier permeability for drug delivery to the brain in a non-human primate. J. Control. Release *336*, 105–111. https://doi.org/10.1016/j.jconrel.2021.06.009.

12. On, N.H., Kiptoo, P., Siahaan, T.J., and Miller, D.W. (2014). Modulation of blood-brain barrier permeability in mice using synthetic E-cadherin peptide. Mol. Pharm. *11*, 974–981. https://doi.org/10.1021/mp400624v.

13. Godinho, B.M.D.C., Henninger, N., Bouley, J., Alterman, J.F., Haraszti, R.A., Gilbert, J.W., Sapp, E., Coles, A.H., Biscans, A., Nikan, M., et al. (2018). Transvascular Delivery of Hydrophobically Modified siRNAs: Gene Silencing in the Rat Brain upon Disruption of the Blood-Brain Barrier. Mol. Ther. *26*, 2580–2591. https://doi.org/10.1016/j.ymthe.2018.08.005.

14. Sonabend, A.M., Gould, A., Amidei, C., Ward, R., Schmidt, K.A., Zhang, D.Y., Gomez, C., Bebawy, J.F., Liu, B.P., Bouchoux, G., et al. (2023). Repeated blood–brain barrier opening with an implantable ultrasound device for delivery of albumin-bound paclitaxel in patients with recurrent glioblastoma: a phase 1 trial. Lancet Oncol. *24*, 509–522. https://doi.org/10.1016/S1470-2045(23)00112-2.

15. Lao, Y.H., Ji, R., Zhou, J.K., Snow, K.J., Kwon, N., Saville, E., He, S., Chauhan, S., Chi, C.W., Datta, M.S., et al. (2023). Focused ultrasound-mediated brain genome editing. Proc. Natl. Acad. Sci. USA *120*, e2302910120. https://doi.org/10.1073/pnas.2302910120.

16. Kofoed, R.H., Dibia, C.L., Noseworthy, K., Xhima, K., Vacaresse, N., Hynynen, K., and Aubert, I. (2022). Efficacy of gene delivery to the brain using AAV and ultrasound depends on serotypes and brain areas. J. Control. Release *351*, 667–680. https://doi.org/10.1016/j.jconrel.2022.09.048.

17. Kwak, G., Grewal, A., Slika, H., Mess, G., Li, H., Kwatra, M., Poulopoulos, A., Woodworth, G.F., Eberhart, C.G., Ko, H.S., et al. (2024). Brain Nucleic Acid Delivery and Genome Editing via Focused Ultrasound-Mediated Blood–Brain Barrier Opening and Long-Circulating Nanoparticles. ACS Nano *18*, 24139–24153. https://doi.org/10.1021/acsnano.4c05270.

18. Zhao, Y.L., Song, J.N., and Zhang, M. (2014). Role of caveolin-1 in the biology of the blood-brain barrier. Rev. Neurosci. *25*, 247–254. https://doi.org/10.1515/revneuro-2013-0039.

19. Sorets, A.G., Rosch, J.C., Duvall, C.L., and Lippmann, E.S. (2020). Caveolae-mediated transport at the injured blood–brain barrier as an underexplored pathway for central nervous system drug delivery. Curr. Opin. Chem. Eng. *30*, 86–95. https://doi.org/10.1016/j.coche.2020.08.009.

20. Tylawsky, D.E., Kiguchi, H., Vaynshteyn, J., Gerwin, J., Shah, J., Islam, T., Boyer, J.A., Boué, D.R., Snuderl, M., Greenblatt, M.B., et al. (2023). P-selectin-targeted nanocarriers induce active crossing of the blood–brain barrier via caveolin-1-dependent transcytosis. Nat. Mater. *22*, 391–399. https://doi.org/10.1038/s41563-023-01481-9.

21. Lei, S., Li, J., Yu, J., Li, F., Pan, Y., Chen, X., Ma, C., Zhao, W., and Tang, X. (2023). Porphyromonas gingivalis bacteremia increases the permeability of the blood-brain barrier via the Mfsd2a/Caveolin-1 mediated transcytosis pathway. Int. J. Oral Sci. *15*, 3. https://doi.org/10.1038/s41368-022-00215-y.

22. Salimi, H., Cain, M.D., Jiang, X., Roth, R.A., Beatty, W.L., Sun, C., Klimstra, W.B., Hou, J., and Klein, R.S. (2020). Encephalitic Alphaviruses Exploit Caveola-Mediated Transcytosis at the Blood-Brain Barrier for Central Nervous System Entry. mBio *11*, 10–1128. https://doi.org/10.1128/mBio.

23. Andreone, B.J., Chow, B.W., Tata, A., Lacoste, B., Ben-Zvi, A., Bullock, K., Deik, A.A., Ginty, D.D., Clish, C.B., and Gu, C. (2017). Blood-Brain Barrier Permeability Is Regulated by Lipid Transport-Dependent Suppression of Caveolae-Mediated Transcytosis. Neuron *94*, 581–594.e5. https://doi.org/10.1016/j.neuron.2017.03.043.

24. Chang, J.H., Greene, C., Frudd, K., Araujo dos Santos, L., Futter, C., Nichols, B.J., Campbell, M., and Turowski, P. (2022). Methamphetamine enhances caveolar transport of therapeutic agents across the rodent blood-brain barrier. Cell Rep. Med. *3*, 100497. https://doi.org/10.1016/j.xcrm.2021.100497.

25. Pandit, R., Koh, W.K., Sullivan, R.K.P., Palliyaguru, T., Parton, R.G., and Götz, J. (2020). Role for caveolin-mediated transcytosis in facilitating transport of large cargoes into the brain via ultrasound. J. Control. Release *327*, 667–675. https://doi.org/10.1016/j.jconrel.2020.09.015.

26. Rotolo, L., Vanover, D., Bruno, N.C., Peck, H.E., Zurla, C., Murray, J., Noel, R.K., O'Farrell, L., Araínga, M., Orr-Burks, N., et al. (2023). Species-agnostic polymeric formulations for inhalable messenger RNA delivery to the lung. Nat. Mater. *22*, 369–379. https://doi.org/10.1038/s41563-022-01404-0.

27. Rui, Y., Wilson, D.R., Tzeng, S.Y., Yamagata, H.M., Sudhakar, D., Conge, M., Berlinicke, C.A., Zack, D.J., Tuesca, A., and Green, J.J. (2022). High-throughput and high-content bioassay enables tuning of polyester nanoparticles for cellular uptake, endosomal escape, and systemic in vivo delivery of mRNA. Sci. Adv. *8*, eabk2855. https://doi.org/10.1126/sciadv.abk2855.

28. Rodrigues, A.F., Rebelo, C., Simões, S., Paulo, C., Pinho, S., Francisco, V., and Ferreira, L. (2023). A Polymeric Nanoparticle Formulation for Targeted mRNA Delivery to Fibroblasts. Adv. Sci. *10*, e2205475. https://doi.org/10.1002/advs.202205475.

29. Mangraviti, A., Tzeng, S.Y., Kozielski, K.L., Wang, Y., Jin, Y., Gullotti, D., Pedone, M., Buaron, N., Liu, A., Wilson, D.R., et al. (2015). Polymeric nanoparticles for nonviral gene therapy extend brain tumor survival in vivo. ACS Nano *9*, 1236–1249. https://doi.org/10.1021/nn504905q.

30. Gao, L., Shi, C., Yang, Z., Jing, W., Han, M., Zhang, J., Zhang, C., Tang, C., Dong, Y., Liu, Y., et al. (2023). Convection-enhanced delivery of nanoencapsulated gene locoregionally yielding ErbB2/Her2-specific CAR-macrophages for brainstem glioma immunotherapy. J. Nanobiotechnol. *21*, 56. https://doi.org/10.1186/s12951-023-01810-9.

31. Mastorakos, P., Zhang, C., Song, E., Kim, Y.E., Park, H.W., Berry, S., Choi, W.K., Hanes, J., and Suk, J.S. (2017). Biodegradable brain-penetrating DNA nanocomplexes and their use to treat malignant brain tumors. J. Control. Release *262*, 37–46. https://doi.org/10.1016/j.jconrel.2017.07.009.

32. Ariful Islam, M., Park, T.E., Firdous, J., Li, H.S., Jimenez, Z., Lim, M., Choi, J.W., Yun, C.H., and Cho, C.S. (2022). Essential cues of engineered polymeric materials regulating gene transfer pathways. Prog. Mater. Sci. *128*, 100961. https://doi.org/10.1016/j.pmatsci.2022.100961.

33. Reshma G, B., Miglani, C., Pal, A., and Ganguli, M. (2024). Sugar alcohol-modified polyester nanoparticles for gene delivery via selective caveolae-mediated endocytosis. Nanoscale *16*, 4114–4124. https://doi.org/10.1039/d3nr05300h.

34. Kaczmarek, J.C., Patel, A.K., Rhym, L.H., Palmiero, U.C., Bhat, B., Heartlein, M.W., DeRosa, F., and Anderson, D.G. (2021). Systemic delivery of mRNA and DNA to the lung using polymer-lipid nanoparticles. Biomaterials *275*, 120966. https://doi.org/10.1016/j.biomaterials.2021.120966.

35. Hirano, A., Kawanami, T., and Llena, J.F. (1994). Electron Microscopy of the Blood-Brain Barrier in Disease. Microsc. Res. Tech. *27*, 543–556.

36. Burks, S.R., Kersch, C.N., Witko, J.A., Pagel, M.A., Sundby, M., Muldoon, L.L., Neuwelt, E.A., Frank, J.A., and Holtzman, D.M. (2021). Blood-brain barrier opening by intracarotid artery hyperosmolar mannitol induces sterile inflammatory and innate immune responses. Proc. Natl. Acad. Sci. USA *118*, e2021915118. https://doi.org/10.1073/pnas.2021915118.

37. Zhang, J., Cai, X., Dou, R., Guo, C., Tang, J., Hu, Y., Chen, H., and Chen, J. (2023). Poly(β-amino ester)s-based nanovehicles: Structural regulation and gene delivery. Mol. Ther. Nucleic Acids *32*, 568–581. https://doi.org/10.1016/j.omtn.2023.04.019.

38. Ayloo, S., and Gu, C. (2019). Transcytosis at the blood–brain barrier. Curr. Opin. Neurobiol. *57*, 32–38. https://doi.org/10.1016/j.conb.2018.12.014.

39. Villaseñor, R., Lampe, J., Schwaninger, M., and Collin, L. (2019). Intracellular transport and regulation of transcytosis across the blood–brain barrier. Preprint at Birkhauser Verlag AG. Cell. Mol. Life Sci. *76*, 1081–1092. https://doi.org/10.1007/s00018-018-2982-x.

40. Lilius, T.O., Mortensen, K.N., Deville, C., Lohela, T.J., Stæger, F.F., Sigurdsson, B., Fiordaliso, E.M., Rosenholm, M., Kamphuis, C., Beekman, F.J., et al. (2023). Glymphatic-assisted perivascular brain delivery of intrathecal small gold nanoparticles. J. Control. Release *355*, 135–148. https://doi.org/10.1016/j.jconrel.2023.01.054.

41. Burger, C., Nguyen, F.N., Deng, J., and Mandel, R.J. (2005). Systemic mannitol-induced hyperosmolality amplifies rAAV2-mediated striatal transduction to a greater extent than local co-infusion. Mol. Ther. *11*, 327–331. https://doi.org/10.1016/j.ymthe.2004.08.031.

42. McCarty, D.M., DiRosario, J., Gulaid, K., Muenzer, J., and Fu, H. (2009). Mannitol-facilitated CNS entry of rAAV2 vector significantly delayed the neurological disease progression in MPS IIIB mice. Gene Ther. *16*, 1340–1352. https://doi.org/10.1038/gt.2009.85.

43. Eltoukhy, A.A., Chen, D., Alabi, C.A., Langer, R., and Anderson, D.G. (2013). Degradable terpolymers with alkyl side chains demonstrate enhanced gene delivery potency and nanoparticle stability. Adv. Mater. *25*, 1487–1493. https://doi.org/10.1002/adma.201204346.

44. Wilson, S.C., Baryza, J.L., Reynolds, A.J., Bowman, K., Keegan, M.E., Standley, S.M., Gardner, N.P., Parmar, P., Agir, V.O., Yadav, S., et al. (2015). Real time measurement of PEG shedding from lipid nanoparticles in serum via NMR spectroscopy. Mol. Pharm. *12*, 386–392. https://doi.org/10.1021/mp500400k.

45. Barker, S.J., Thayer, M.B., Kim, C., Tatarakis, D., Simon, M., Dial, R.L., Nilewski, L., Wells, R.C., Zhou, Y., Afetian, M., et al. (2024). Targeting Transferrin Receptor to Transport Antisense Oligonucleotides Across the Blood-Brain Barrier. Sci. Transl. Med. *16*, eadi2245. https://doi.org/10.1101/2023.04.25.538145.

46. Okuyama, T., Eto, Y., Sakai, N., Nakamura, K., Yamamoto, T., Yamaoka, M., Ikeda, T., So, S., Tanizawa, K., Sonoda, H., and Sato, Y. (2021). A Phase 2/3 Trial of Pabinafusp Alfa, IDS Fused with Anti-Human Transferrin Receptor Antibody, Targeting Neurodegeneration in MPS-II. Mol. Ther. *29*, 671–679. https://doi.org/10.1016/j.ymthe.2020.09.039.

47. Gu, Y., Cai, R., Zhang, C., Xue, Y., Pan, Y., Wang, J., and Zhang, Z. (2019). MiR-132-3p boosts caveolae-mediated transcellular transport in glioma endothelial cells by

targeting PTEN/PI3K/PKB/Src/Cav-1 signaling pathway. FASEB J. *33*, 441–454. https://doi.org/10.1096/fj.201800095RR.

48. Ju, X., Miao, T., Chen, H., Ni, J., and Han, L. (2021). Overcoming Mfsd2a-Mediated Low Transcytosis to Boost Nanoparticle Delivery to Brain for Chemotherapy of Brain Metastases. Adv. Healthc. Mater. *10*, e2001997. https://doi.org/10.1002/adhm.202001997.

49. Ben-Akiva, E., Karlsson, J., Hemmati, S., Yu, H., Tzeng, S.Y., Pardoll, D.M., and Green, J.J. (2023). Biodegradable lipophilic polymeric mRNA nanoparticles for ligand-free targeting of splenic dendritic cells for cancer vaccination. Proc. Natl. Acad. Sci. USA *120*, e2301606120. https://doi.org/10.1073/pnas.2301606120.

50. Cheng, Q., Wei, T., Farbiak, L., Johnson, L.T., Dilliard, S.A., and Siegwart, D.J. (2020). Selective organ targeting (SORT) nanoparticles for tissue-specific mRNA delivery and CRISPR–Cas gene editing. Nat. Nanotechnol. *15*, 313–320. https://doi.org/10.1038/s41565-020-0669-6.

51. Dilliard, S.A., and Siegwart, D.J. (2023). Passive, active and endogenous organ-targeted lipid and polymer nanoparticles for delivery of genetic drugs. Nat. Rev. Mater. *8*, 282–300. https://doi.org/10.1038/s41578-022-00529-7.

52. Grigsby, C.L., and Leong, K.W. (2010). Balancing protection and release of DNA: Tools to address a bottleneck of non-viral gene delivery. J. R. Soc. Interface *7*, 67–82. https://doi.org/10.1098/rsif.2009.0260.

53. Park, T.E., Kang, B., Kim, Y.K., Zhang, Q., Lee, W.S., Islam, M.A., Kang, S.K., Cho, M.H., Choi, Y.J., and Cho, C.S. (2012). Selective stimulation of caveolae-mediated endocytosis by an osmotic polymannitol-based gene transporter. Biomaterials *33*, 7272–7281. https://doi.org/10.1016/j.biomaterials.2012.06.037.

54. Cadiz, M.P., Jensen, T.D., Sens, J.P., Zhu, K., Song, W.M., Zhang, B., Ebbert, M., Chang, R., and Fryer, J.D. (2022). Culture shock: microglial heterogeneity, activation, and disrupted single-cell microglial networks in vitro. Mol. Neurodegener. *17*, 26. https://doi.org/10.1186/s13024-022-00531-1.

55. Joseph, A., Liao, R., Zhang, M., Helmbrecht, H., McKenna, M., Filteau, J.R., and Nance, E. (2020). Nanoparticle-microglial interaction in the ischemic brain is modulated by injury duration and treatment. Bioeng. Transl. Med. *5*, e10175. https://doi.org/10.1002/btm2.10175.

56. Gao, J., Xia, Z., Gunasekar, S., Jiang, C., Karp, J.M., and Joshi, N. (2024). Precision drug delivery to the central nervous system using engineered nanoparticles. Nat. Rev. Mater. *9*, 567–588. https://doi.org/10.1038/s41578-024-00695-w.

57. Finneran, D.J., Njoku, I.P., Flores-Pazarin, D., Ranabothu, M.R., Nash, K.R., Morgan, D., and Gordon, M.N. (2021). Toward Development of Neuron Specific Transduction After Systemic Delivery of Viral Vectors. Front. Neurol. *12*, 685802. https://doi.org/10.3389/fneur.2021.685802.

58. Wilson, D.R., Mosenia, A., Suprenant, M.P., Upadhya, R., Routkevitch, D., Meyer, R.A., Quinones-Hinojosa, A., and Green, J.J. (2017). Continuous microfluidic assembly of biodegradable poly(Beta-amino ester)/DNA nanoparticles for enhanced gene delivery. J. Biomed. Mater. Res. *105*, 1813–1825. https://doi.org/10.1002/jbm.a.36033.